molecules

MDPI

Communication

Supramolecular Diiodine-Bromostannate(IV) Complexes: Narrow Bandgap Semiconductors

Nikita A. Korobeynikov, Andrey N. Usoltsev, Pavel A. Abramov, Maxim N. Sokolov and Sergey A. Adonin *

Nikolaev Institute of Inorganic Chemistry SB RAS, 630090 Novosibirsk, Russia; 27041998rus@gmail.com (N.A.K.); usoltsev@niic.nsc.ru (A.N.U.); abramov@niic.nsc.ru (P.A.A.); caesar@niic.nsc.ru (M.N.S.)
* Correspondence: adonin@niic.nsc.ru

Abstract: Three supramolecular bromostannates(IV) with "trapped" diiodine molecules, $Cat_2\{[SnBr_6](I_2)\}$ (Cat = Me_4N^+ (**1**), 1-$MePy^+$ (**2**) and 4-MePyH (**3**)), were synthesized. In all cases, I_2 linkers are connected with bromide ligands via halogen···halogen non-covalent interactions. Articles **1–3** were studied using Raman spectroscopy, thermogravimetric analysis, and diffuse reflectance spectroscopy. The latter indicates that **1–3** are narrow band gap semiconductors.

Keywords: polyhalogens; halogen bonding; non-covalent interactions; tin; halide complexes; iodine

check for updates

Citation: Korobeynikov, N.A.; Usoltsev, A.N.; Abramov, P.A.; Sokolov, M.N.; Adonin, S.A. Supramolecular Diiodine-Bromostannate(IV) Complexes: Narrow Bandgap Semiconductors. *Molecules* **2022**, *27*, 3859. https://doi.org/10.3390/molecules27123859

Academic Editor: Antonio Caballero

Received: 15 May 2022
Accepted: 9 June 2022
Published: 16 June 2022

1. Introduction

Metal halide complexes, or halometalates, represent the class of coordination compounds which, apart from fundamental interest (in particular, related to structural chemistry), attracts attention due to numerous areas of materials science where they can be applied. Those include design of ferroelectric and ferroelastic materials [1–5], photocatalysis [6–8], luminescence [9–15], photochromism [16,17], etc. However, the most prominent area is photovoltaics. Since it was discovered that 3D perovskite-type iodoplumbates(II) can be used as light absorbers in solar cells, this area has experienced very rapid growth [18–27] (according to Scopus data, the number of papers on this topic dramatically increases annually). In the last few years, there appear many works about the use of iodometalates of p-block metals other than lead (this is driven mostly by environmental considerations). Among the elements considered for this purpose, there are bismuth, tin, antimony, etc. [28]. Yet, performance of solar cells based thereupon is significantly lower than for iodoplumbate(II) derivatives but, at the same time, it was found that iodometalates(III) (M = Sb, Bi) can serve as a component of highly efficient photodetectors [29–34]. This fact strongly inspires further research in this field.

It is commonly assumed that the main disadvantage of halometalates other than Pb(II) and Sn(II) derivatives in the course of photovoltaic applications is their stereochemistry. While iodoplumbates(II) and –stannates(II) can form isotropic, covalently-bonded 3D structures (perovskite-type), this is impossible for Sb(III) and Bi(III), which usually form discrete, 1D or, rarely, 2D anions [35]. For M(IV) halide complexes, it is even more challenging since they most commonly appear as mononuclear $[MX_6]^{2-}$ anions. A possible strategy to overcome this problem is the use of supramolecular approaches (increasing of dimensionality via non-covalent interactions in a solid state). One of such ideas presented recently is the use of supramolecular polyhalogen-halometalate hybrids. Incorporation of di- or polyiodide units into a structure commonly yields a narrower optical band gap of resulting compounds [36,37] and the assembly of 1D, 2D, or even 3D associates via halogen bond [38]. Recent examples of diiodo-bromoantimonates(III) and –bromotellurates(IV) demonstrate [39,40] that such hybrids indeed can serve as components of photodetectors. Therefore, a search of new compounds belonging to this family is well justified.

Although tin(IV) halide complexes feature stereochemistry almost identical to Te(IV), corresponding polyiodo-halometalates have yet been unknown. In this work, we present

the first examples of this class: $Cat_2\{[SnBr_6](I_2)\}$ (cat = $Me4N^+$ (**1**), 1-$MePy^+$ (**2**) and 4-$MePyH^+$ (**3**). In addition to the structural studies, we hereby report their thermal stability, optical properties, and Raman spectra.

2. Experimental Part

All reagents were obtained from commercial sources and used and purchased. 1-methylpyridinium iodide (1-MePyI) was prepared by reaction of pyridine and 1.1× excess of methyl iodide. Elemental analysis was performed on a Euro NA 3000 Elemental analyzer (EuroVector, Pavia, Italy). In all cases, concentrated aqueous HBr was used.

2.1. Synthesis of 1

An amount of 60 mg (0.22 mmol) of $SnBr_2$ was dissolved in 3 mL of HBr at 70 °C. Then, 100 mg (0.43 mmol) of I_2 were added. After 15 min, a solution of Me_4Br in 2 mL of HBr was added. The hot mixture was filtered, slowly cooled to r.t., and then to 5 °C. Within 6 h, dark cherry-red crystals of **1** were formed. The yield was 65%. Element analysis calculated for $C_8H_{24}N_2SnBr_6I_2$: C 9.64; H 2.43; N 2.81. Found: C 9.74; H 2.51; N 2.90.

2.2. Synthesis of 2

An amount of 192 mg (0.87 mmol) of 1-MePyI was dissolved in 4 mL of water and mixed with a stoichiometric amount of $AgNO_3$ with stirring. After filtering off the formed AgI, the resulting solution was evaporated and the precipitate was dissolved in 4 mL of HBr. The mixture was heated to 70 °C. After that, 120 mg (0.43 mmol) $SnBr_2$ and 220 mg (0.87 mmol) of I_2 were added. After cooling the solution, it was kept at 5 °C for one day, resulting in dark cherry-red crystals of **2**. Yield: 67%. Element analysis calculated for $C_{12}H_{16}N_2SnBr_6I_2$: C 13.91; H 1.56; N 2.70. Found: C 14.00; H 1.61; N 2.78.

2.3. Synthesis of 3

An amount of 120 mg (0.43 mmol) of $SnBr_2$ was dissolved in 4 mL of HBr. The solution was heated to 70 °C; 220 mg (0.87 mmol) of I_2 was added and the mixture was stirred for 30 min. After that, 85 µL (0.87 mmol) of 4-MePy were added. The mixture was cooled to r.t., then to 5 °C. After 7 h, dark cherry-red crystals of **3** formed. The estimated yield was 63%. Element analysis calculated for $C_{12}H_{16}N_2SnBr_6$: C 18.43; H 2.06; N 3.58. Found: C 18.38; H 2.13; N 3.57.

2.4. X-ray Diffractometry

Crystallographic data and refinement details for **1–3** are given in Table S1 (SI). The diffraction data were collected on a New Xcalibur (Agilent Technologies, Santa Clara, CA, USA) diffractometer with MoKα radiation (λ = 0.71073) by doing φ scans of narrow (0.5°) frames at 150 K. Absorption correction was done empirically using SCALE3 ABSPACK (CrysAlisPro, Agilent Technologies, Version 1.171.37.35 (release 13-08-2014 CrysAlis171.NET) (compiled 13 August 2014, 18:06:01)).

Structures were solved by SHELXT [41] and refined by full-matrix least-squares treatment against $|F|^2$ in anisotropic approximation with SHELX 2014/7 [42] in ShelXle program [43]. H-atoms were refined in the geometrically calculated positions. The main geometrical parameters are summarized in Table S2.

The structure of 1 was refined in $I4_1cd$ as an inversion twin with BASF 0.48. PLATON did not suggest any symmetry change. Attempts to solve the structure in $I4_1/acd$ or $P4_2nm$ space groups did not give any improvements. One position of highly disordered CH_3 group around N3 was not refined due to the absence of q-peaks with right geometry. Splitting and refinement of C-atoms generated based on found positions were unstable. The occupancy of N3 was 100%. The refinement composition was $C_{7.75}H_{23.25}Br_6I_2N_2Sn$. The elemental analysis data confirmed the complex composition as $C_8H_{24}Br_6I_2N_2Sn$. According to the electron density distribution, the second position of $[SnBr_6]^{2-}$ octahedral unit with ≈8% occupancy has been found (see SI for details).

The crystallographic data have been deposed in the Cambridge Crystallographic Data Centre under the deposition codes CCDC 2170497-2170499.

2.5. Raman Spectroscopy

Raman spectra were collected using a LabRAM HR Evolution (Horiba) spectrometer with the excitation by the 633 nm line of the He-Ne laser. The spectra at room temperatures were obtained in the backscattering geometry with a Raman microscope. The laser beam was focused to a diameter of 2 μm using a LMPlan FL 50×/0.50 Olympus objective. The spectral resolution was 0.7 cm^{-1}. The laser power on the sample surface was about 0.03 mW.

2.6. Diffuse Reflectance Spectroscopy

Diffuse reflectance spectra were measured on a setup which consisted of a Kolibri-2 spectrometer (VMK Optoelektronica, Novosibirsk, Russia), fiber optic cable QR-400-7 (Ocean Optics, Rochester, NY, USA), and deuterium–tungsten lamp AvaLight-DHS (Avantes, Apeldoorn, The Netherlands). The reference of 100% reflectance was BaSO4 powder. The spectra were recorded five times in the wavelength interval of 300–1000 nm and then averaged to reduce the random error.

2.7. Thermogravimetric Analysis (TGA)

TGA were carried out on a TG 209 F1 Iris thermobalance (NETZSCH, Selb, Germany). The measurements were made in a helium flow in the temperature range of 30–450 °C using the heating rate of 10 °C min^{-1}, the gas flow rate of 60 mL min^{-1}, and open Al crucibles.

2.8. Powder X-ray Diffractometry (PXRD)

XRD analysis of polycrystals was performed on a Shimadzu XRD-7000 diffractometer (CuK-alpha radiation, Ni—filter, linear One Sight detector, 5–50° 2θ range, 0.0143° 2θ step, 2 s per step). Plotting of PXRD patterns and data treatment was performed using X'Pert Plus software (see SI).

3. Results and Discussion

Synthesizing complexes **1–3**, we used the same "straightforward" approach [39,40] as we extensively applied earlier for Bi(III), Sb(V), and Te(IV) complexes: a solution containing anionic bromometalate complex anions was mixed with I_2 and then with the salt of the organic cation. The choice of the latter is known to play the most important role in halometalate chemistry since the nature of the cation has a very strong influence on the system of non-covalent interactions in solid state and, therefore, it affects the assembly of polynuclear anions. However, very little is known about rational principles of precursor selection—in other words, screening is yet the most common strategy in halometalate chemistry. On this reason, we chose highly available cations which we already used in our earlier works on polyhalogen-halometalates.

The XRD data indicate that, like in halotellurates(IV), all isolated complexes are built out of mononuclear $[SnBr_6]^{2-}$ anions. The Sn-Br bond lengths are 2.587–2.645 Å in **1**, 2.563–2.627 Å in **2**, and 2.563–2.684 Å in **3**, respectively. The composition of the polyhalogeno-anionic part in all cases is identical: $\{[SnBr_6](I_2)\}$. The I···I bonds in **1–3** are 2.692–2.695, 2.703, and 2.686 Å, respectively.

In **1**, the I_2 units are disordered over two positions with 0.985:0.015 occupancies. The $[SnBr_6]^{2-}$ units form non-covalent interactions with I_2 (for most populated I_2 positions, corresponding Br···I are 3.201–3.203 Å which is less than the sum of corresponding Bondi's van der Waals radii (3.81 Å [44,45]). The I-I-Br angles are 170.57–173.88°. The superposition of $\{[SnBr_6](I_2)\}$ chains can be considered as a pseudo-2D substructure (Figure 1). The positional disorder of $[SnBr_6]^{2-}$ over two closed positions (0.92/0.08 occupancies) was found in the crystal structure of **1** (Figure S3, SI). Such complex anions interact with I_2 molecules, producing layers where both components follow 44 plane net topology (Figure S4). Such layers stack together in ABABA . . . manner (Figure S5) with shifting in a

[110] crystal direction. Both $[SnBr_6]^{2-}$ and I_2 centers of gravity follow bcc sublattices. TMA cations occupy voids between the above-mentioned layers (Figure S6). There are three types of TMA cations in the unit cell (Figure S7): the first and second types occupy special positions and the third type occupies common positions. Cations of the latter type have non-linear periodicity.

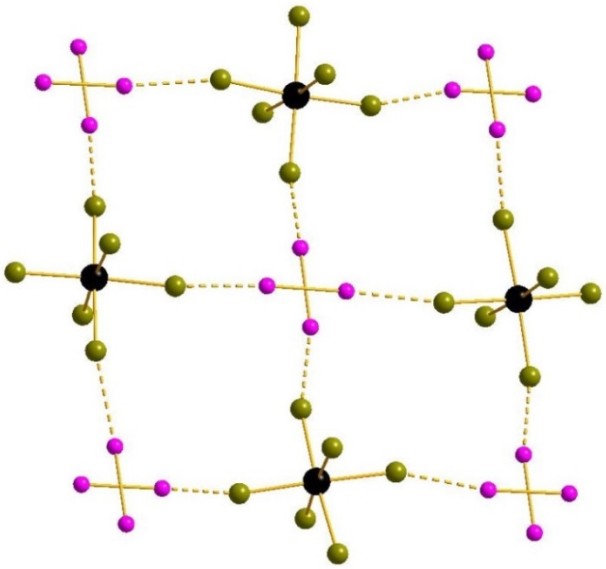

Figure 1. Supramolecular associates built of $[SnBr_6]^{2-}$ and I_2 units in the structure of **1**. Here and below: Sn black, Br olive-green, I purple, I···Br interactions dashed. All positions of disordered I_2 fragments are shown.

In both **2** and **3**, I_2 and $[SnBr_6]^{2-}$ structural units form linear supramolecular chains (Figure 2). The I···Br distances in **2** and **3** are 3.219 and 3.412–3.432 Å, the Sn-Br-I and Br-I-I angles are 143.46 and 173.03 in **2**, 160.00–167.09 and 162.67–170.18°, respectively.

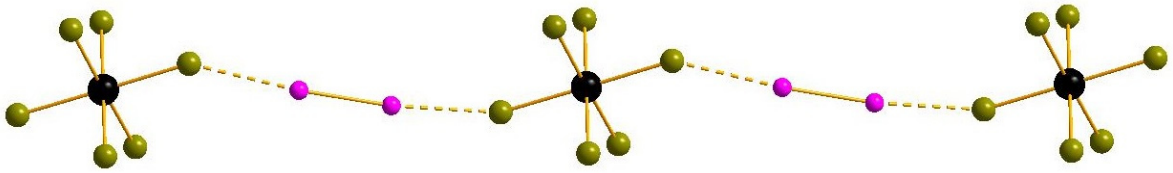

Figure 2. Linear $\{[SnBr_6](I_2)\}^{2n-}$ associates in the structures of **2** and **3**.

In **2**, there are two types of above-mentioned 1D chains running perpendicular to each other along [b − a] and [b + a] directions, respectively (Figure S7, SI). In the crystal, packing such 1D structures can be combined into pseudo layers located in the [110] crystal direction. These layers stack together with AABBAA . . . topology. 1-methylpyridinium cations are located in the space between the above-mentioned 1D associates. In **3**, $[SnBr_6]^{2-}$ and I_2 form chains running along [010] the crystal direction. In the crystal packing (Figure S8), such associates can be combined into pseudo layers located in [110] the crystal direction. These layers stack together, producing ABABA . . . topology. 4-methylpyridinium cations are located in the space between the above-mentioned 1D structures. Hence, changing of the Me-group position strongly affects the crystal packing topology of isolated compounds.

Complex **3** demonstrates poor stability while being isolated from I_2-containing mother liquor. It decomposes within a few dozen minutes, losing incorporated I_2 (elemental analysis for the residue corresponds to "diiodine-free" $(4\text{-MePyH})_2[SnBr_6]$). Both **1** and **2** are stable and they were isolated as single phases, as follows from PXRD data (see SI, Figures S1 and S2). Nevertheless, we succeeded in recording of Raman spectra for the whole series of samples. Results are presented on Figure 3. It can be noticed that in each case,

there are two bands within the 180–200 cm^{-1} region where I_2 has a highly characteristic band in diiodo-halometalates [46]. Most likely, the bands at 196–200 cm^{-1} are related to I_2 while those at 182–184 correspond to $[SnBr_6]^{2-}$ vibrations [47] (as well as all bands at wavelengths < 150 cm^{-1}; these data agree well with our previous work [48]).

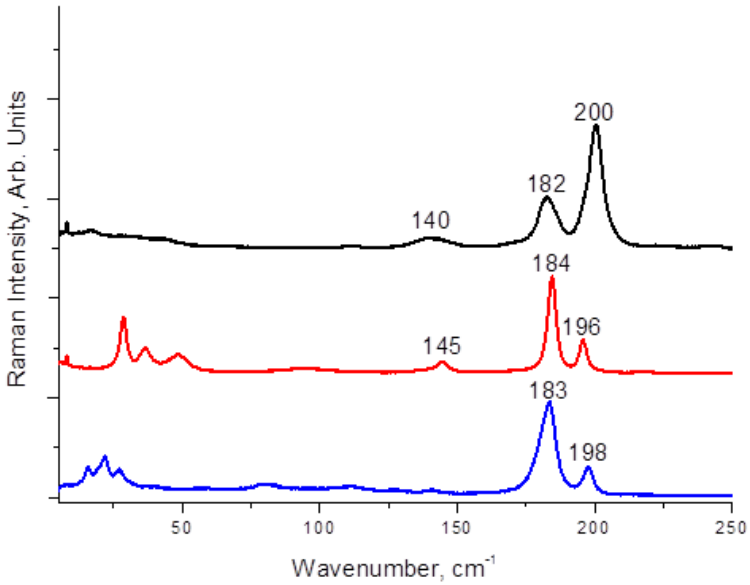

Figure 3. Raman spectra of **1** (black), red (**2**), and blue (**3**).

As follows from TGA data, **1** and **2** demonstrate different thermal stability—decomposition corresponding to continuous loss of diiodine occurs at >110 and >90 °C, respectively (Figures 4 and 5). These results agree well with our observations made for diiodo-bromotellurates(IV) [40]: depending on the nature of the organic cation and, therefore, on the system of EH···X interactions it forms in solid state with halide ligands and poly-halogeno units, stability can be dramatically diverse.

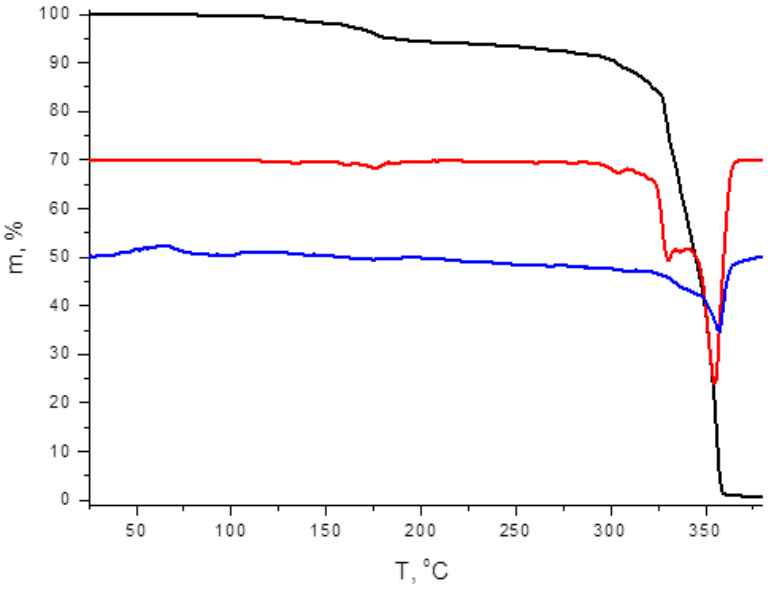

Figure 4. TG, DTG, and DTA curves of **1**.

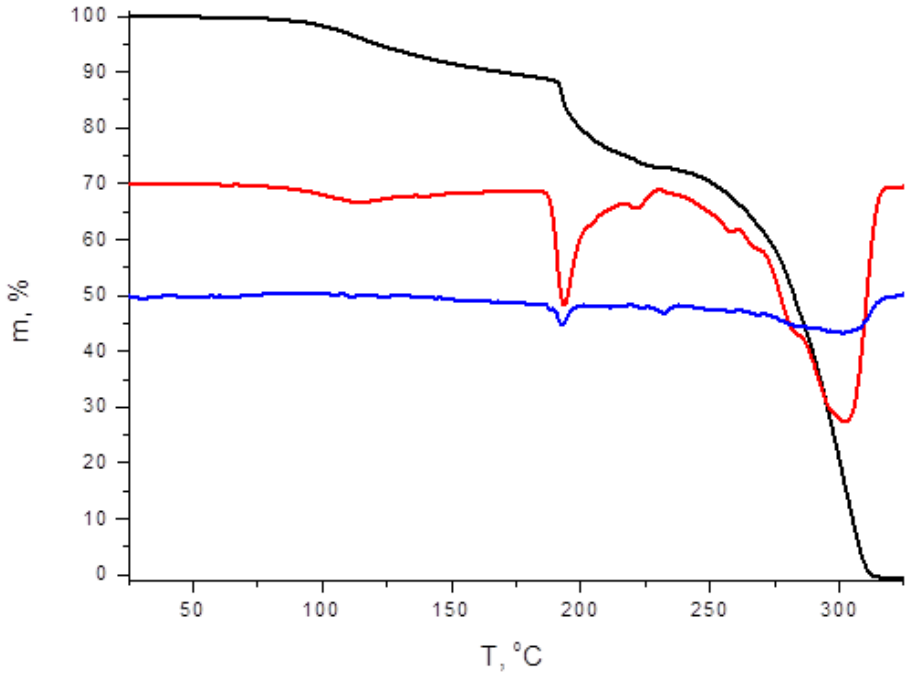

Figure 5. TG, DTG, and DTA curves of **2**.

Diffuse reflectance spectra of **1** and **2** are presented in Figures 6 and 7. The optical band gaps for these two complexes are 1.68 and 1.69 eV, respectively, which is more than for similar diiodo-bromotellurates described by us earlier (1.41–1.74, with average 1.55 eV [40]). The overall features of these spectra are quite common for p-block halometalates [49,50].

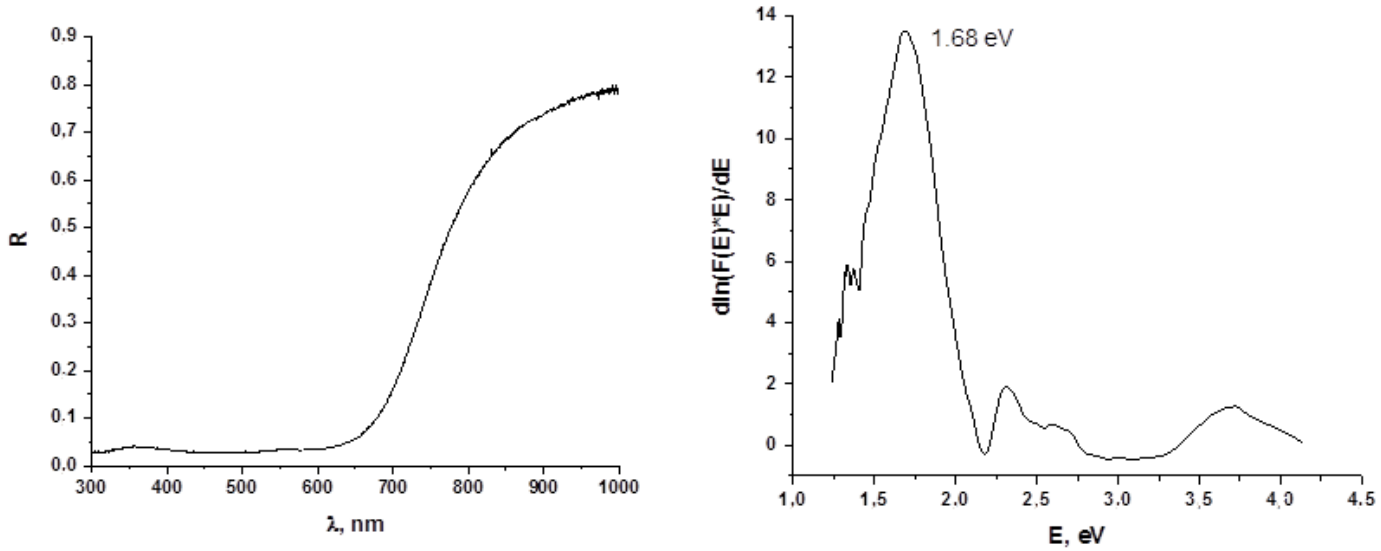

Figure 6. Diffuse reflectance spectrum (**left**) and optical band gap determination (Tauc coordinates, **right**) for **1**.

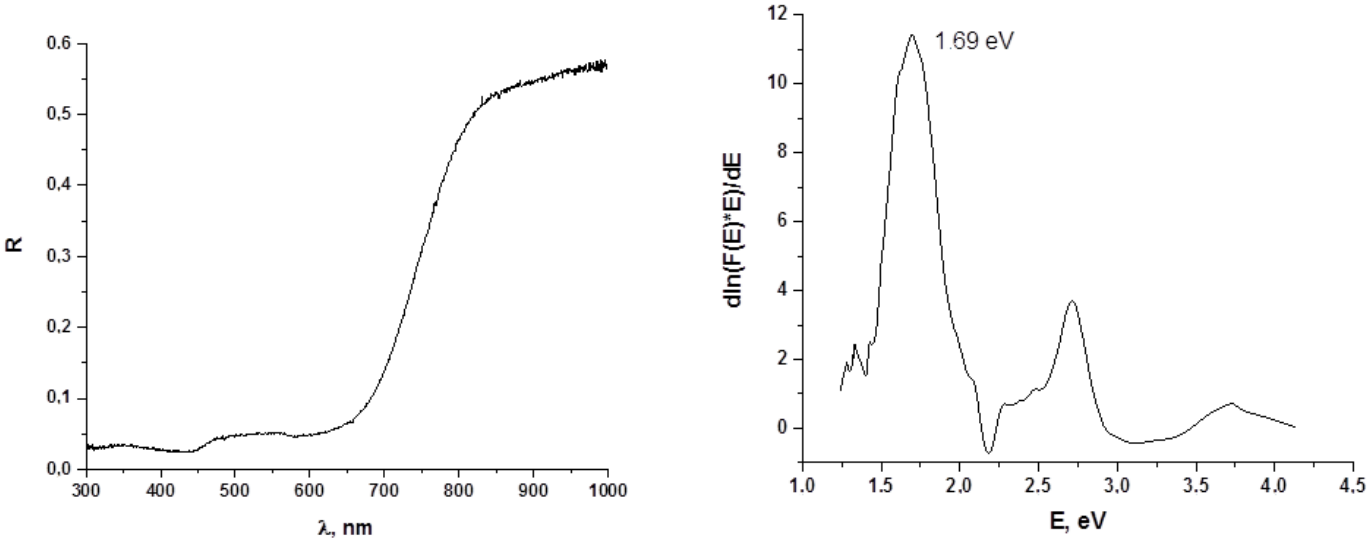

Figure 7. Diffuse reflectance spectrum (**left**) and optical band gap determination (Tauc coordinates, **right**) for **2**.

4. Conclusions

This work demonstrates that the general strategy utilized in preparation of polyhalogen-halometalates, designed and widely applied by us for synthesis of Bi(III), Te(IV), and Sb(V) complexes, as well as dichloro-chlorostannates(IV) and –plumbates(IV) [51], works very well for diiodo-bromostannates(IV). We assume the existence of such hybrids of other metals commonly forming mononuclear halometalate anions $[MX_6]^{2-}$, such as Zr, Hf, Ir, etc. Corresponding experiments are underway in our group.

Supplementary Materials: The following supporting information can be downloaded at: https://www.mdpi.com/article/10.3390/molecules27123859/s1, Figure S1: Calculated (black) and experimental (red) PXRD patterns of **1**; Figure S2: Calculated (black) and experimental (red) PXRD patterns of **2**; Figure S3: Positional disordering of $[SnBr_6]^{2-}$ octahedron over two closed positions with 0.92 (red) and 0.08 (blue) occupancies; Figure S4: Structure of the layer formed by $[SnBr_6]^{2-}$ and I2 units; Figure S5: Layered crystal packing of **1**; Figure S6: Positions of TMA+ cations in the void between {$[SnBr_6]^{2-}$ + I2} nets; Figure S7: Crystal packing of **2**; Figure S8. Crystal packing of **3**; Table S1: Experimental details; Table S2: Selected geometric parameters (Å).

Author Contributions: Conceptualization, S.A.A. and M.N.S.; methodology, S.A.A.; validation, P.A.A. and A.N.U.; formal analysis, S.A.A. and P.A.A.; investigation, N.A.K. and P.A.A.; resources, S.A.A.; data curation, A.N.U.; writing—original draft preparation, S.A.A., A.N.U., P.A.A., and M.N.S.; writing—review and editing, M.N.S.; visualization, N.A.K. and S.A.A.; supervision, M.N.S. and S.A.A.; project administration, S.A.A.; funding acquisition, S.A.A. All authors have read and agreed to the published version of the manuscript.

Funding: This research was funded by Russian Science Foundation, Grant No. 18-73-10040, and partially supported by Ministry of Science and Higher Education of the Russian Federation (spectral characterization of the samples, 121031700313-8).

Institutional Review Board Statement: Not applicable.

Informed Consent Statement: Not applicable.

Data Availability Statement: Not applicable.

Conflicts of Interest: The authors declare no conflict of interest.

Sample Availability: Not available.

References

1. Przesławski, J.; Piecha-Bisiorek, A.; Jakubas, R. Specific heat anomaly in ferroelectric: Bis(imidazolium) pentachloroantimonate(III) $(C_3N_2H_5)_2[SbCl_5]$. *J. Mol. Struct.* **2016**, *1110*, 97–101. [CrossRef]
2. Mencel, K.; Kinzhybalo, V.; Jakubas, R.; Zaręba, J.K.; Szklarz, P.; Durlak, P.; Drozd, M.; Piecha-Bisiorek, A. 0D Bismuth (III)-Based Hybrid Ferroelectric: Tris (acetamidinium) Hexabromobismuthate (III). *Chem. Mater.* **2021**, *33*, 8591–8601. [CrossRef]
3. Piecha, A.; Białońska, A.; Jakubas, R. Structure and ferroelectric properties of $[C_3N_2H_5]_5[Bi_2Br_{11}]$. *J. Phys. Condens. Matter* **2008**, *20*, 325224. [CrossRef]
4. Owczarek, M.; Szklarz, P.; Jakubas, R. Towards ferroelectricity-inducing chains of halogenoantimonates(iii) and halogenobismuthates(iii). *RSC Adv.* **2021**, *11*, 17574–17586. [CrossRef] [PubMed]
5. Szklarz, P.; Jakubas, R.; Medycki, W.; Gągor, A.; Cichos, J.; Karbowiak, M.; Bator, G. $(C_3N_2H_5)_3Sb_2I_9$ and $(C_3N_2H_5)_3Bi_2I_9$: Ferroelastic lead-free hybrid perovskite-like materials as potential semiconducting absorbers. *Dalt. Trans.* **2022**, *51*, 1850–1860. [CrossRef] [PubMed]
6. Lei, X.-W.; Yue, C.-Y.; Feng, L.-J.; Han, Y.-F.; Meng, R.-R.; Yang, J.-T.; Ding, H.; Gao, C.-S.; Wang, C.-Y. Syntheses, crystal structures and photocatalytic properties of four hybrid iodoargentates with zero- and two-dimensional structures. *CrystEngComm* **2015**, *18*, 427–436. [CrossRef]
7. Lei, X.-W.; Yue, C.-Y.; Zhao, J.-Q.; Han, Y.-F.; Yang, J.-T.; Meng, R.-R.; Gao, C.-S.; Ding, H.; Wang, C.-Y.; Chen, W.-D. Low-Dimensional Hybrid Cuprous Halides Directed by Transition Metal Complex: Syntheses, Crystal Structures, and Photocatalytic Properties. *Cryst. Growth Des.* **2015**, *15*, 5416–5426. [CrossRef]
8. Lei, X.-W.; Yue, C.-Y.; Wei, J.-C.; Li, R.-Q.; Mi, F.-Q.; Li, Y.; Gao, L.; Liu, Q.-X. Novel 3D Semiconducting Open-Frameworks based on Cuprous Bromides with Visible Light Driven Photocatalytic Properties. *Chem. A Eur. J.* **2017**, *23*, 14547–14553. [CrossRef]
9. Feng, L.-J.; Zhao, Y.-Y.; Song, R.-Y.; Lei, X.-W. Three homologous 1D lead halide perovskites with broadband white-light emissions. *Inorg. Chem. Commun.* **2021**, *136*, 109146. [CrossRef]
10. Zhao, J.-Q.; Shi, H.-S.; Zeng, L.-R.; Ge, H.; Hou, Y.-H.; Wu, X.-M.; Yue, C.-Y.; Lei, X.-W. Highly emissive zero-dimensional antimony halide for anti-counterfeiting and confidential information encryption-decryption. *Chem. Eng. J.* **2021**, *431*, 134336. [CrossRef]
11. Ahern, J.C.; Nicholas, A.; Kelly, A.W.; Chan, B.; Pike, R.D.; Patterson, H.H. A terbium chlorobismuthate(III) double salt: Synthesis, structure, and photophysical properties. *Inorganica Chim. Acta* **2018**, *478*, 71–76. [CrossRef]
12. Kelly, A.W.; Nicholas, A.; Ahern, J.; Chan, B.; Patterson, H.H.; Pike, R. Alkali metal bismuth(III) chloride double salts. *J. Alloys Compd.* **2016**, *670*, 337–345. [CrossRef]
13. Heine, J.; Wehner, T.; Bertermann, R.; Steffen, A.; Müller-Buschbaum, K. $^2{}_\infty[Bi_2Cl_6(pyz)_4]$: A 2D-pyrazine coordination polymer as soft host lattice for the luminescence of the lanthanide ions Sm^{3+}, Eu^{3+}, Tb^{3+}, and Dy^{3+}. *Inorg. Chem.* **2014**, *53*, 7197–7203. [CrossRef]
14. Dehnhardt, N.; Klement, P.; Chatterjee, S.; Heine, J. Divergent Optical Properties in an Isomorphous Family of Multinary Iodido Pentelates. *Inorg. Chem.* **2019**, *58*, 10983–10990. [CrossRef] [PubMed]
15. Jing, C.-Q.; Yin, X.; Xiao, P.-C.; Gao, Y.-J.; Wu, X.-M.; Yue, C.-Y.; Lei, X.-W. Bulk Mn^{2+} Doped 1D Hybrid Lead Halide Perovskite with Highly Efficient, Tunable and Stable Broadband Light Emissions. *Chem. A Eur. J.* **2022**, *28*, e202103043. [CrossRef]
16. Lin, R.-G.; Xu, G.; Lu, G.; Wang, M.-S.; Li, P.-X.; Guo, G.-C. Photochromic hybrid containing in situ-generated benzyl viologen and novel trinuclear $[Bi_3Cl_{14}]^{5-}$: Improved photoresponsive behavior by the $\pi\cdots\pi$ interactions and size effect of inorganic oligomer. *Inorg. Chem.* **2014**, *53*, 5538–5545. [CrossRef]
17. Toma, O.; Mercier, N.; Botta, C. N-Methyl-4, 4′-bipyridinium and N-Methyl-N′-oxide-4, 4′-bipyridinium Bismuth Complexes–Photochromism and Photoluminescence in the Solid State. *Eur. J. Inorg. Chem.* **2013**, *2013*, 1113–1117. [CrossRef]
18. Grishko, A.Y.; Zharenova, E.A.; Goodilina, E.A.; Tarasov, A.B. Solvent-free deposition of hybrid halide perovskites onto thin films of copper iodide p-type conductor. *Mendeleev Commun.* **2021**, *31*, 163–165. [CrossRef]
19. Marchenko, E.I.; Fateev, S.A.; Petrov, A.A.; Goodilin, E.A.; Tarasov, A.B. Theoretical assessment of thermodynamic stability of 2D octane-1,8-diammonium lead halide perovskites. *Mendeleev Commun.* **2020**, *30*, 279–281. [CrossRef]
20. Petrov, A.A.; Fateev, S.A.; Zubavichus, Y.V.; Dorovatovskii, P.V.; Khrustalev, V.N.; Zvereva, I.A.; Petrov, A.V.; Goodilin, E.A.; Tarasov, A.B. Methylammonium polyiodides: Remarkable phase diversity of the simplest and low-melting alkylammonium polyiodide system. *J. Phys. Chem. Lett.* **2019**, *10*, 5776–5780. [CrossRef]
21. Elnaggar, M.M.; Frolova, L.A.; Gordeeva, A.M.; Ustinova, M.I.; Laurenzen, H.; Akkuratov, A.V.; Nikitenko, S.L.; Solov'eva, E.A.; Luchkin, S.Y.; Fedotov, Y.S.; et al. Improving stability of perovskite solar cells using fullerene-polymer composite electron transport layer. *Synth. Met.* **2022**, *286*, 117028. [CrossRef]
22. Udalova, N.N.; Fateev, S.A.; Nemygina, E.M.; Zanetta, A.; Grancini, G.; Goodilin, E.A.; Tarasov, A.B. Nonmonotonic Photostability of $BA_2MA_{n-1}Pb_nI_{3n+1}$ Homologous Layered Perovskites. *ACS Appl. Mater. Interfaces* **2022**, *14*, 961–970. [CrossRef] [PubMed]
23. Frolova, L.A.; Gutsev, L.G.; Ramachandran, B.R.; Dremova, N.N.; Aldoshin, S.M.; Troshin, P.A. Exploring $CsPbI_3$–FAI alloys: Introducing low-dimensional $Cs_2FAPb_2I_7$ absorber for efficient and stable perovskite solar cells. *Chem. Eng. J.* **2021**, *426*, 131754. [CrossRef]
24. Petrov, A.A.; Ordinartsev, A.A.; Fateev, S.A.; Goodilin, E.A.; Tarasov, A.B. Solubility of Hybrid Halide Perovskites in DMF and DMSO. *Molecules* **2021**, *26*, 7541. [CrossRef] [PubMed]

25. Mangrulkar, M.; Luchkin, S.Y.; Akbulatov, A.F.; Zhidkov, I.; Kurmaev, E.Z.; Troshin, P.A.; Stevenson, K.J. Rationalizing the effect of overstoichiometric PbI_2 on the stability of perovskite solar cells in the context of precursor solution formulation. *Synth. Met.* **2021**, *278*, 116823. [CrossRef]
26. Alidaei, M.; Ahmadi, V.; Mousavi, S.M.; Roghabadi, F.A. Stability improvement of perovskite solar cell using photoswitchable and moisture resistant dual-function interfacial layer. *J. Alloys Compd.* **2022**, *903*, 163891. [CrossRef]
27. Oniy Aghmiuni, K.; Arabpour Roghabadi, F.; Rezvani, H.; Alidaei, M.; Falahi, M.; Pashaei Soorbaghi, F.; Ahmadi, V. The Future of Hybrid and Inorganic Perovskite Materials: Technology Forecasting. *Energy Technol.* **2021**, *9*, 2100376. [CrossRef]
28. Ganose, A.M.; Savory, C.N.; Scanlon, D.O. Beyond methylammonium lead iodide: Prospects for the emergent field of ns^2 containing solar absorbers. *Chem. Commun.* **2016**, *53*, 20–44. [CrossRef]
29. Usoltsev, A.N.; Elshobaki, M.; Adonin, S.A.; Frolova, L.A.; Derzhavskaya, T.; Abramov, P.A.; Anokhin, D.V.; Korolkov, I.V.; Luchkin, S.Y.; Dremova, N.N.; et al. Polymeric iodobismuthates $[Bi_3I_{10}]$ and $[BiI_4]$ with N-heterocyclic cations: Promising perovskite-like photoactive materials for electronic devices. *J. Mater. Chem. A* **2019**, *7*, 5957–5966. [CrossRef]
30. Han, L.; Wang, P.; Wang, Z.; Liu, Y.; Zheng, Z.; Cheng, H.; Huang, B. Zero-dimensional hydrazine iodobismuthate as a lead-free perovskite-like light absorber in a self-powered photodetector. *J. Alloys Compd.* **2021**, *893*, 162347. [CrossRef]
31. Lai, Z.; Wang, F.; Meng, Y.; Bu, X.; Kang, X.; Quan, Q.; Wang, W.; Yip, S.P.; Liu, C.; Ho, J.C. Solution-processed lead-free double perovskite microplatelets with enhanced photoresponse and thermal stability. *Sci. China Mater.* **2022**, *65*, 1313–1319. [CrossRef]
32. Shuang, Z.; Zhou, H.; Wu, D.; Zhang, X.; Xiao, B.; Ma, G.; Zhang, J.; Wang, H. Low-temperature process for self-powered lead-free $Cs_2AgBiBr_6$ perovskite photodetector with high detectivity. *Chem. Eng. J.* **2022**, *433*, 134544. [CrossRef]
33. Li, L.; Ye, G.; Luo, T.; Chen, X.; Zhang, G.; Wu, H.; Yang, L.; Zhang, W.; Chang, H. Centimeter-Sized Stable Zero-Dimensional $Cs_3Bi_2I_9$ Single Crystal for Mid-Infrared Lead-Free Perovskite Photodetector. *J. Phys. Chem. C* **2022**, *126*, 3646–3652. [CrossRef]
34. Mei, J.; Liu, M.; Vivo, P.; Pecunia, V. Two-Dimensional Antimony-Based Perovskite-Inspired Materials for High-Performance Self-Powered Photodetectors. *Adv. Funct. Mater.* **2021**, *31*, 2106295. [CrossRef]
35. Wu, L.-M.; Wu, X.-T.; Chen, L. Structural overview and structure–property relationships of iodoplumbate and iodobismuthate. *Coord. Chem. Rev.* **2009**, *253*, 2787–2804. [CrossRef]
36. Shestimerova, T.A.; Golubev, N.A.; Yelavik, N.A.; Bykov, M.A.; Grigorieva, A.V.; Wei, Z.; Dikarev, E.V.; Shevelkov, A.V. Role of I_2 Molecules and Weak Interactions in Supramolecular Assembling of Pseudo-Three-Dimensional Hybrid Bismuth Polyiodides: Synthesis, Structure, and Optical Properties of Phenylenediammonium Polyiodobismuthate(III). *Cryst. Growth Des.* **2018**, *18*, 2572–2578. [CrossRef]
37. Shestimerova, T.A.; Yelavik, N.A.; Mironov, A.V.; Kuznetsov, A.N.; Bykov, M.A.; Grigorieva, A.V.; Utochnikova, V.V.; Lepnev, L.S.; Shevelkov, A.V. From isolated anions to polymer structures through linking with i2: Synthesis, structure, and properties of two complex bismuth(III) iodine iodides. *Inorg. Chem.* **2018**, *57*, 4077–4087. [CrossRef]
38. Usoltsev, A.N.; Korobeynikov, N.A.; Novikov, A.S.; Plyusnin, P.E.; Kolesov, B.A.; Fedin, V.P.; Sokolov, M.N.; Adonin, S.A. One-Dimensional Diiodine—Iodobismuthate(III) Hybrids $Cat_3[Bi_2I_9](I_2)_3$: Syntheses, Stability, and Optical Properties. *Inorg. Chem.* **2020**, *59*, 17320–17325. [CrossRef]
39. Adonin, S.A.; Udalova, L.I.; Abramov, P.A.; Novikov, A.S.; Yushina, I.V.; Korolkov, I.V.; Semitut, E.Y.; Derzhavskaya, T.A.; Stevenson, K.J.; Troshin, P.A.; et al. A Novel Family of Polyiodo-Bromoantimonate(III) Complexes: Cation-Driven Self-Assembly of Photoconductive Metal-Polyhalide Frameworks. *Chem. A Eur. J.* **2018**, *24*, 14707–14711. [CrossRef]
40. Novikov, A.V.; Usoltsev, A.N.; Adonin, S.A.; Bardin, A.A.; Samsonenko, D.G.; Shilov, G.V.; Sokolov, M.N.; Stevenson, K.J.; Aldoshin, S.M.; Fedin, V.P.; et al. Tellurium complex polyhalides: Narrow bandgap photoactive materials for electronic applications. *J. Mater. Chem. A* **2020**, *8*, 21988–21992. [CrossRef]
41. Sheldrick, G.M. SHELXT—Integrated space-group and crystal-structure determination. *Acta Crystallogr. Sect. A Found. Adv.* **2015**, *A71*, 3–8. [CrossRef] [PubMed]
42. Sheldrick, G.M. Crystal structure refinement with SHELXL. *Acta Crystallogr. Sect. C Struct. Chem.* **2015**, *C71*, 3–8. [CrossRef] [PubMed]
43. Hübschle, C.B.; Sheldrick, G.M.; Dittrich, B. ShelXle: A Qt graphical user interface for SHELXL. *J. Appl. Crystallogr.* **2011**, *44*, 1281–1284. [CrossRef] [PubMed]
44. Bondi, A. van der Waals Volumes and Radii of Metals in Covalent Compounds. *J. Phys. Chem.* **1966**, *70*, 3006–3007. [CrossRef]
45. Mantina, M.; Chamberlin, A.C.; Valero, R.; Cramer, C.J.; Truhlar, D.G. Consistent van der Waals radü for the whole main group. *J. Phys. Chem. A* **2009**, *113*, 5806–5812. [CrossRef]
46. Adonin, S.A.; Usoltsev, A.N.; Novikov, A.S.; Kolesov, B.A.; Fedin, V.P.; Sokolov, M.N. One- And Two-Dimensional Iodine-Rich Iodobismuthate(III) Complexes: Structure, Optical Properties, and Features of Halogen Bonding in the Solid State. *Inorg. Chem.* **2020**, *59*, 3290–3296. [CrossRef]
47. Tudela, D.; Khan, M.A. Tin-bromine bond lengths and Mössbauer quadrupole splittings of tin(IV) bromide complexes. Crystal structure of pyridinium tetrabromodiphenylstannate(IV). *J. Chem. Soc. Dalt. Trans.* **1991**, 1003–1006. [CrossRef]
48. Korobeynikov, N.A.; Usoltsev, A.N.; Abramov, P.A.; Novikov, A.S.; Sokolov, M.N.; Adonin, S.A. Bromine-rich tin(IV) halide complexes: Experimental and theoretical examination of Br···Br noncovalent interactions in crystalline state. *Polyhedron* **2022**, *222*, 115912. [CrossRef]

49. Goforth, A.M.; Tershansy, M.A.; Smith, M.D.; Peterson, L.; Kelley, J.G.; DeBenedetti, W.J.I.; zur Loye, H.-C. Structural Diversity and Thermochromic Properties of Iodobismuthate Materials Containing d-Metal Coordination Cations: Observation of a High Symmetry $[Bi_3I_{11}]^{2-}$ Anion and of Isolated I^- Anions. *J. Am. Chem. Soc.* **2011**, *133*, 603–612. [CrossRef]
50. Shayapov, V.R.; Usoltsev, A.N.; Adonin, S.A.; Sokolov, M.N.; Samsonenko, D.G.; Fedin, V.P. Thermochromism of bromotellurates(iv): Experimental insights. *New J. Chem.* **2019**, *43*, 3927–3930. [CrossRef]
51. Usoltsev, A.N.; Korobeynikov, N.A.; Kolesov, B.A.; Novikov, A.S.; Samsonenko, D.G.; Fedin, V.P.; Sokolov, M.N.; Adonin, S.A. Rule, Not Exclusion: Formation of Dichlorine-Containing Supramolecular Complexes with Chlorometalates(IV). *Inorg. Chem.* **2021**, *60*, 4171–4177. [CrossRef] [PubMed]